SEMI-PHYSICAL SIMULATION RESEARCH ON THE CONTROL SYSTEM OF COMBINE HARVESTER CUTTING TABLE
/
联合收割机割台控制系统的半实物仿真研究

Yihu WANG[1], Guohai ZHANG[2*], Xipeng QIAN[1], Qian DONG[1]
[1] Shandong University of Technology, Zibo 255200, China;
[2] Institute of Modern Agricultural Equipment, Shandong University of Technology, Zibo 255200, China;
E-mail: guohaizhang@sdut.edu.cn

ABSTRACT

To address challenges in developing the rice-wheat harvester cutting platform controller—such as sensitivity to working conditions, long development cycles, and cumbersome performance testing—a semi-physical simulation platform is designed. Based on the functional requirements of the cutting platform, Simulink is used to build a mathematical model of the controller and its I/O hardware model. A hardware-in-the-loop simulation test platform is developed using the TC377ECU controller. By integrating the Whale Optimization PID algorithm, overshoot is reduced by 3.5%, and rise time improves by 0.303 s compared to conventional PID. Testing in both simulation and real environments shows a maximum absolute error of 10.58 mm for cutting height and a correlation coefficient of 0.9474. The rotational speed errors for the reel and auger have expectations of 0.106 rad/min and 0.101 rad/min, with standard deviations of 0.165 rad/min and 0.172 rad/min. This validates the controller's feasibility, shortens development time, and lowers costs.

摘要

针对稻麦收获机割台控制器开发过程受工况影响较大，传统开发过程周期长，测试控制器性能过程繁琐等问题，设计了一套稻麦收获机割台自动调控系统半实物仿真平台。以稻麦收获机割台功能需求作为开发指标，利用 simulink 搭建控制器数学模型以及 I/O 硬线模型，基于 TC377ECU 控制器搭建硬件在环仿真测试平台。结合鲸鱼优化 PID 算法对控制策略进行了优化，相较于普通 PID，超调量降低了 3.5%，上升时间提升了 0.303s。通过仿真平台与真实环境进行试验对比，割台高度的最大绝对误差是 10.58mm，相关系数为 0.9474；拨禾轮和搅龙转速误差的数学期望依次为 0.106 rad/min 和 0.101 rad/min，标准差为 0.165 rad/min 和 0.172 rad/min，测试了控制器和仿真平台的可行性，缩短了开发周期，降低了开发成本。

INTRODUCTION

As one of China's major food crops, ensuring the production of rice and wheat is of primary importance. In 2024, 23,090.7 thousand hectares of wheat were sown, marking an increase of 31.7 thousand hectares, or 0.1%. With the growing prevalence of machine harvesting across the country, the automation level of agricultural machinery has reached a point where higher standards are required. This makes the development and optimization of agricultural machinery functions increasingly significant. To overcome the limitations of using joysticks for regulating the cutting platform parameters in traditional harvesters, researchers have increasingly focused on developing automatic regulation systems for the cutting platform of grain combine harvesters. *Ji et al., (2023),* employed the polar filling method to model the rigid and flexible discrete elements of reed stalks, and conducted a three-point bending test in EDEM software to calibrate the bonding parameters. The optimal parameter combinations for the cutting table were identified through simulation analysis and later verified by field tests, confirming their alignment with the simulation results. *Yao et al., (2023),* investigated the impact of harvester forward speed, transverse cutter cutting height, and longitudinal cutter cutting speed on the cutting table loss rate in rapeseed combine harvesting, addressing the issue of high loss rates. The analysis revealed that the significance order of these factors was: cutting speed > forward speed > cutting height. Optimal parameter combinations were determined through response surface analysis and regression model optimization, with the results experimentally verified for reliability.

Aiming to address the issues of low gripping capacity, poor cutting quality, and easy damage of existing harvester tools, *Zhao et al., (2024),* designed a bionic knife blade inspired by the maxillary teeth of ants. They investigated the effects of parameters such as blade tooth pitch, constructed edge angle, and tilt angle on the stress field and deformation through finite element analysis. The results confirmed that optimizing the knife edge design significantly enhances its performance, providing a theoretical foundation for the design of harvester knives.

Chen et al., (2018), addressed the low automation levels in cutting platform parameter regulation by using a PLC as the controller to design an automatic adjustment device for the rice combine harvester's cutting platform. In their system, the response time for controlling the rotational speed of the reel was ≤ 0.8 s, with a control accuracy of 91.5%.

Liu et al., (2022), designed an adaptive profiling cutting table to ensure the stubble height remains within an optimal range during harvesting. The table could adjust its height and level adaptively, using a PLC controller and a fuzzy PID method for regulation. The cutting table's rising speed was 0.216 m/s, and its descending speed was 0.244 m/s.

Ji et al., (2022), aimed to improve harvesting quality by designing a cutting table with a response time of ≤ 0.8 s and control accuracy of 91.5%. They also developed a device to match the rotational speed of the reel with the forward speed using an STM32 controller and fuzzy PID control strategy. This system could adapt to different crops, with a rotational speed-to-vehicle speed ratio between 1.4 and 1.8, yielding better harvesting results.

Shi et al., (2024), designed an adaptive control system for the cutting platform to address the inefficiency and inaccuracy of manual adjustments. Using a PLC as the controller, the system achieved an average response time of 2.3 s for height control. These studies demonstrate that factors such as the height of the cutting platform, reel height, rotational speed of the reel, and auger speed directly affect the harvesting loss rate of rice and wheat. However, most of the research primarily focuses on optimizing the regulation process of the reel using fuzzy PID methods for height and speed control. The optimization of cutting platform regulation strategies remains under developed. Moreover, the process of controller development and testing requires numerous experiments for validation. This not only increases the risk of actuator burnout due to errors in control strategies but also raises testing costs and demands frequent mounting, dismounting, and optimization operations. Additionally, given the growth cycles of rice and wheat, continuous field experiments are necessary for verification, resulting in a lengthy development cycle. HIL simulation allows for effective testing of controllers by simulating realistic controlled objects. While HIL simulation has been widely applied in industries such as automotive and aviation, *Shahir et al., (2021),* uses HIL to test complex algorithms in electric vehicle propulsion architectures, validating the correctness of the proposed theoretical concepts.

Abboush et al., (2024), applies semi-physical simulation techniques for fault injection, testing the safety of automobiles. *Klionovska et al., (2021),* utilizes the HIL technique for spacecraft rendezvous simulation testing. Its application in agriculture has only emerged relatively recently, primarily for tractor steering control and gearshift simulation, *Hang et al., (2024),* improves the steering control strategy for tractors and develop HIL testbeds. *Cevallos et al., (2022),* applies the HIL technique to validate a hybrid control method for a greenhouse model.

Wu et al., (2023), uses HIL technology for an electric tractor seeding unit, building a hardware-in-the-loop simulation testbed to compare and validate proposed improvement strategies. *Zhu et al., (2022),* applies the HIL technique to a corn harvester threshing unit, creating a low loss intelligent control simulation platform for corn.

Zhai et al., (2023), establishes a semi-physical simulation test platform for the tractor electro hydraulic suspension control system, verifying the performance of the designed controller in this system. It is evident that the introduction of semi-physical simulation technology has accelerated the development of automation in the agricultural sector, yet its application in the development of cutting table regulation systems remains limited.

Therefore, this paper aims to optimize the cutting platform's automatic regulation system, addressing the gap in current research regarding the optimization of cutting platform height control strategies. By combining the Whale Optimization Algorithm (WOA) with a PID based control strategy for height regulation, this approach reduces overshoot by 3.5% compared to traditional PID control, thereby enhancing system stability. Additionally, the rise time is improved by 0.303 seconds, which boosts the system's response speed. Agricultural automation systems are often influenced by environmental changes and the aging of equipment, which can impact response speed.

However, the WOA-optimized controller demonstrates strong adaptability to these variations, enhancing the system's robustness. In terms of reel and auger speed regulation, this study integrates findings from existing research to ensure that the speed ratio between the reel and vehicle speed remains within an optimal range. The TC377 is selected as the control center for the system, offering better compatibility with the harvester. To address the long testing cycles in traditional development processes, a semi-physical simulation platform for the cutting platform's automatic control system is constructed. The feasibility of the platform is evaluated in comparison with traditional methods, providing a solid foundation for the continued development of the cutting platform control system.

MATERIALS AND METHODS
Simulation platform overall structure

The overall structure of the simulation platform should have the function of simulating the environment of the real vehicle, so it is necessary to analyze the overall architecture of the cutting platform first; as shown in Figure 1, the whole simulation platform consists of on-board controllers, driver operating system, hydraulic model, actuator model, operation interface, information processing system, and power supply module, the on-board controller as the core component of the whole system. The simulation platform board issues its input to simulate the voltage signal of the sensor so that the controller mistakenly thinks that the current working environment is the real machine, to achieve the purpose of testing the controller function. The data transmission between the controller and the simulation platform is via I/O hardwire. The CAN communication bus and the current value of each data can be monitored in real-time via telegrams. The operator interface interacts with the information processing system to send user operation data and controller feedback results. Its functional design mainly includes the working mode selection of the whole machine, the height of the cutting platform, the height of the reel, the speed regulation and monitoring of the reel, and the entire regulation process is realized by the controller sending out PWM pulse signals to control the openness of the solenoid valve.
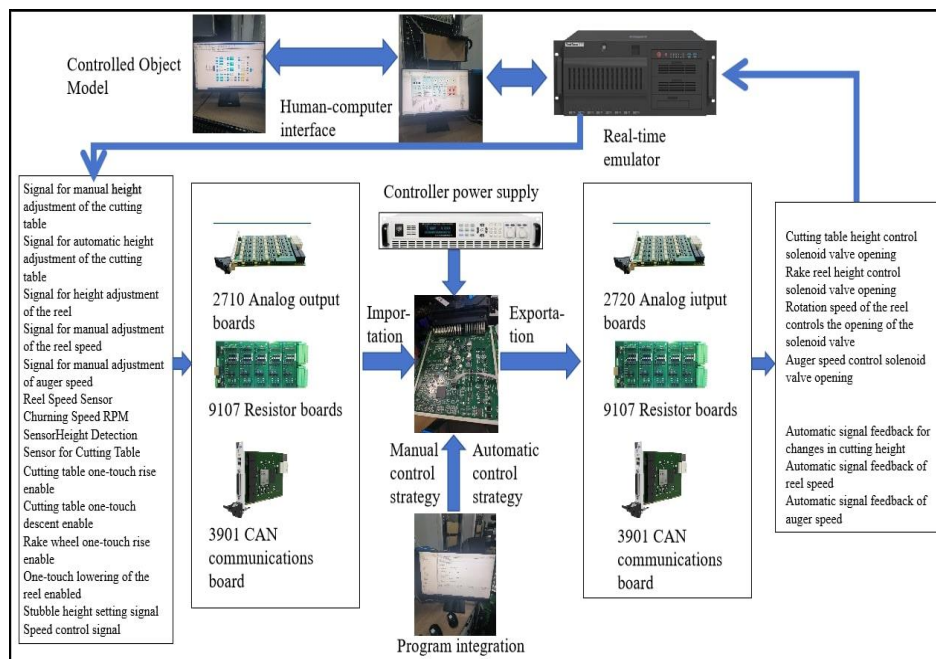

Fig. 1 - Block diagram of grain harvester cutting platform control system components

A complete grain harvester cutting table model is established using existing experimental data and formulas to create a realistic test environment for the controller. This includes simulating the conventional vehicle voltage signals required by the controller, the voltage signals from the cutter sensors, the control signals from the receiver controller, and the feedback status signals. The input and output signals of the entire system are regulated by the real-time simulator, and the regulation strategy is implemented based on the established I/O model. The controlled variables include the cutting platform height, the reel's height and rotational speed, and the auger's rotational speed. Modeling of the actuator based on the hydraulic system, with its schematic diagram shown in Figure 2.
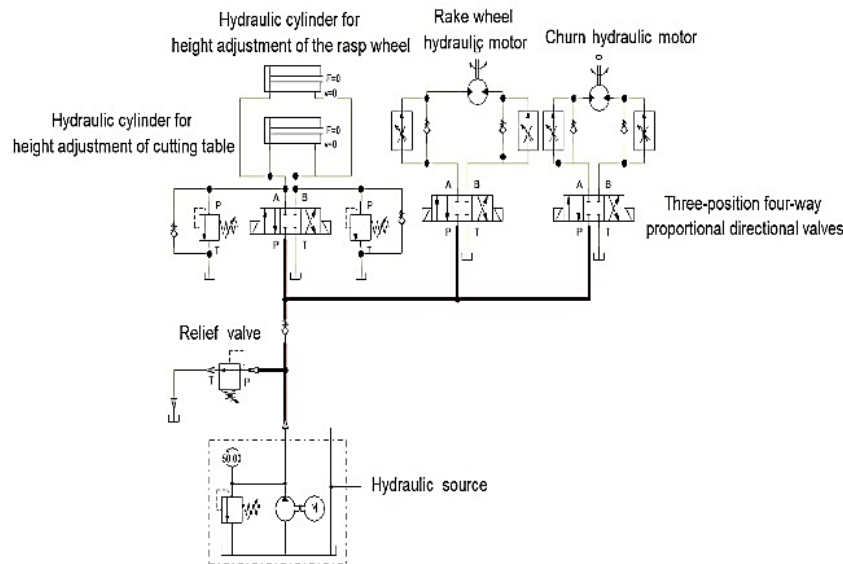
Fig. 2 - Hydraulic system schematic

The complete model must account for the following considerations: ①The hydraulic element's power source is the pressure generated by fluid flow, requiring incorporation of the nonlinear relationship between flow rate and pressure. ②Assuming the hydraulic oil is compressible, the mechanical analysis must include the elastic resistance of the liquid. ③To ensure compatibility with the controller and minimize computational burden, the model must be discretized.

The height regulation of the cutting platform is primarily achieved by controlling the expansion and contraction of the hydraulic cylinder. The hydraulic cylinder's power is derived from the conversion of hydraulic oil flow, and the displacement of the hydraulic cylinder is determined through the mathematical relationship between pressure and acceleration. A piston pump model is selected as the power source for the entire hydraulic system, with its displacement formula given by:

$$V=\frac{\pi}{4}d^2 Dz\eta_v tan\delta \tag{1}$$

where d is the plunger diameter, m; D is the diameter of the distribution circle of the plunger on the cylinder body, m; z is the number of plungers; η_v is the pump volumetric efficiency; δ is the inclination of the swashplate, rad.

Find the flow rate produced by the pump based on the displacement of the piston pump:

$$Q=nV \tag{2}$$

where:

Q is the output flow rate of the piston pump, m³/s; n is the engine speed of the piston pump, r/min; V is the displacement of the piston pump, L/rev.

Hydraulic oil exits the hydraulic pump, with one path flowing through the relief valve into the tank and the other passing through the check valve into the solenoid directional valve. During this process, a localized fixed capacity cavity is formed. Assuming the liquid is compressible, if the volume of the fixed-capacity cavity is V and the initial internal pressure is P_0, then as the liquid continues to flow into the cavity at a changing rate of ΔQ, the pressure inside the cavity can be expressed as follows:

$$P=P_0+B\int\frac{\Delta Q}{V}dt \tag{3}$$

where:

P is the hydraulic chamber pressure in Pa; P_0 is the initial pressure of the hydraulic chamber in Pa; B is the bulk modulus of elasticity of the hydraulic fluid in Pa; ΔQ is the amount of flow change in m³/s; V is the volume of a fixed volume in m³.

The hydraulic fluid output from the check valve serves as the input to the three-position four-way proportional directional valve. The position and opening of the proportional directional valve are controlled by a PWM signal from the controller. Given that the valve port opening is not strictly linear, the flow rate output from each valve port, based on the valve port characteristics, can be expressed as follows:

$$Q=C_d A_0 \sqrt{\frac{2\Delta p}{\rho}} \tag{4}$$

$$A_0 = \begin{cases} 0, & x < x_0, \\ Kx, & x > x_0. \end{cases} \tag{5}$$

C_d is the flow coefficient, dimensionless; A_0 is the cross sectional area of the hole, m²; ρ is the density of the liquid, kg/m³; Δp is the pressure difference between the inlet and outlet of the small hole, m²; x_0 denotes the deadband flow rate, m²; K is the gain coefficient, dimensionless.

The hydraulic oil output by the reversing valve flows to the hydraulic cylinder, and the flow of hydraulic oil realizes the reciprocating motion of the hydraulic cylinder push rod; according to the relationship between the force and acceleration can be calculated the displacement of the hydraulic bar, and its kinetic equation can be expressed as:

$$F_i - F_o - F_c - F_k - F_{load} = ma \tag{6}$$

F_i is the inlet chamber pressure, N; F_o is the outlet pressure, N; F_c is the liquid damping force, N; F_k is the liquid elastic force, N; F_{load} is the model load force, N; m is the mass of the piston rod, kg; a is the piston rod acceleration, m/s².

The RPM model hydraulic circuit is similar to the height model, with the key difference being that the actuator in the RPM model is a hydraulic motor. This motor converts the pressure of the hydraulic fluid into mechanical energy to drive the rotation of the reel. The moment balance equation for the hydraulic motor and the load can be expressed as (*Lu et al., 2023*):

$$D_m(p_H + p_L) = J_t \frac{d^2\theta_m}{dt^2} + B_m \frac{d\theta_m}{dt} + G\theta_m + T_l \tag{7}$$

p_H and p_L are the hydraulic motor inlet chamber pressure and return chamber pressure, respectively, Pa; D_m is the displacement of the hydraulic motor, m³/s; J_t is the total inertia of the hydraulic motor and load, kg·m²; B_m is the viscous damping coefficient, kg/s; G is the load spring stiffness, N·m; T_l is any unintentional load moment acting on the hydraulic motor shaft, N; θ_m is the motor rotation angle, rad.

As the command processing center of the entire platform, the controller's control strategy plays a pivotal role, directly impacting the functionality of the cutting table and the overall effectiveness of the test. Among the various control tasks, height regulation of the cutting table is particularly critical. To achieve fast, stable, and precise control, a PID control strategy optimized using the Whale Optimization Algorithm (WOA) has been selected. WOA is an innovative bio-inspired intelligence algorithm modeled after the foraging behavior of humpback whales (*NadimiShahraki et al., 2021; Miao et al., 2025; Wei et al., 2025*). In the WOA optimization process, each humpback whale represents a candidate solution. These whales utilize a distinctive hunting technique known as the bubble-net predation strategy, which serves as the foundation for the algorithm's search and exploitation mechanisms.

In the encircling prey phase, the current best candidate solution is assumed to be the optimal solution for the target prey, or at least close to it (*Yan et al., 2022*). The humpback whale then moves around this best candidate solution, continuously updating its position. The mathematical model for this phase is represented as:

$$X(t+1) = X^*(t) - A \times |CX^*(t) - X(t)| \tag{8}$$

t is the number of iterations for the current update position, dimensionless; $X^*(t)$ is the current optimal position vector, m; $X(t)$ is the current position vector of the whale, m; A and C are position vector coefficients which operate as follows:

$$A = \frac{2T_{max}}{T_{max} + t}(2r_1 - 1) \tag{9}$$

$$C = 2r_2 \tag{10}$$

r_1 and r_2 is a random vector in the range (0,1), dimensionless; T_{max} is the iteration maximum, dimensionless.

During the prey search phase, humpback whales update their position in an upward spiral and keep approaching their prey, its hunting model is:

$$X(t+1) = X^*(t) + e^{bl}\cos(2\pi l)|X^*(t) - X(t)| \tag{11}$$

b is the whale spiral path coefficient and l is a (0,1) random number conforming to a uniform distribution, dimensionless.

From this, two behaviors of whales when catching prey are derived, assuming that the probability of both behaviors is the same.

$$X(t+1)=\begin{cases} X^*(t)-A\times|CX^*(t)-X(t)|, p<0.5 \\ X^*(t)+e^{bl}\cos(2\pi l)|X^*(t)-X(t)|, p\geq 0.5 \end{cases} \tag{12}$$

where p is the probability of the two behaviors, dimensionless.

When attacking the prey, the difference between the iteration value t and the maximum iteration value gradually decreases, causing the range of values of A to decline. When the value of A is within [-1,1], the next position of the whale can be any position between it and the prey, and at A < 1, the attack is launched at the prey.

To ensure that all humpback whales can perform a thorough search in the solution space, they must randomize their targets based on each other's positions. When the value of A is outside the range of [-1,1], the algorithm randomly selects a whale's position to modify the position vectors of other whales. This helps them locate suitable prey and enables global search capabilities.

$$X(t+1)=X_{random}(t)-A\times|CX_{random}(t)-X(t)| \tag{13}$$

where $X_{random}(t)$ is a vector of randomly selected whale positions, m.

Based on PID control of the cutting table elevation, the system error is used as the evaluation function for the whale optimization algorithm. The fitness function value is calculated, and the proportional, integral, and derivative parameters are adjusted according to the fitness to optimize the PID controller, thereby achieving optimal control.

To reduce the computational load of the simulation platform and facilitate test sampling, the model must be discretized. The Simulink tool is used to automatically solve the discrete model using the forward Euler method, which can be expressed as follows:

$$x(k+1)=x(k)+Tf(x(k),t(k)) \tag{14}$$

where $x(k)$ is the state variable at the current moment k, m; $x(k+1)$ is the state variable at the next moment k+1, m; T is the sampling time, s; $f(x(k),t(k))$ is the derivative of the system, m/s.

RESULTS AND ANALYSIS

The simulation platform functionality test primarily includes the simulation function test of the controller signals and the hardware-in-the-loop (HIL) test.

Taking the cutting platform height regulation signal as an example, the controller adjusts the lift of the hydraulic cylinder based on the detection signal from the profiling device. The profiling device's source is the angle detected by the angle sensor, which sends out a voltage signal. This process can be used as the basis for analog signal testing. The voltage signal value can be set on the control panel, and a multimeter can be used to measure the voltage signal output from the corresponding board to conduct the test.

For the selection of an angle measurement sensor in a cutting table profiling device, the GT-B type Hall angle sensor is a suitable choice. This sensor features an output voltage range of 0-3.3 V, which corresponds linearly to an angular range of 0-360°.

The relationship between the measured angle and the simulated angle value follows the equation:

$$V=a\times\frac{3.3}{360} \tag{15}$$

where: V is the simulation platform voltage setting, V; a is the angle value measured by the true angle sensor, °.

$$\theta=V\times\frac{360}{3.3} \tag{16}$$

where θ is the simulation platform angle analog input value, °.

Based on the measured angle value, the required voltage parameter V can be determined and set on the platform, allowing for the calculation of the corresponding angle input. A comparison between the measured sensor values and the platform's angle measurement values was conducted, with the test results presented in Table 1.

The results indicate that the maximum absolute error between the simulation platform and the measured sensor angle is 0.98°, while the maximum relative error is 0.08°. This discrepancy arises because, after setting the voltage parameter V, the board card outputs the voltage according to the set value, but minor deviations exist in the actual output. This conclusion is further validated by measuring the board card's output voltage using a multimeter.

Table 1

Sensor and simulation platform angle measurements

Experiment number	Measured angular value a	Simulation platform voltage setting value V	Simulation angle value θ	Absolute error	Relative error
	[°]	[V]	[°]	[°]	[-]
1	10.37	0.095	11.15	0.78	0.08
2	10.89	0.990	11.69	0.8	0.07
3	11.03	0.100	11.8	0.77	0.07
4	12.36	0.113	11.38	0.98	0.08
5	13.45	0.123	14.31	0.86	0.06
6	13.91	0.128	13.17	0.74	0.05
7	14.16	0.130	13.38	0.78	0.06
8	14.87	0.136	15.6	0.73	0.05
9	15.34	0.140	16.07	0.73	0.05
10	15.96	0.146	16.74	0.78	0.05

The CAN signal test uses VBA software to monitor real-time changes in message transmission data, assessing the accuracy and timeliness of signal transmission. Figure 3 displays the screen of real-time monitoring during the test. The CAN message monitoring screen displays real-time data transmission between the platform and the controller. The current value of each signal is updated in real-time, simulating an environment where CAN communication is active.
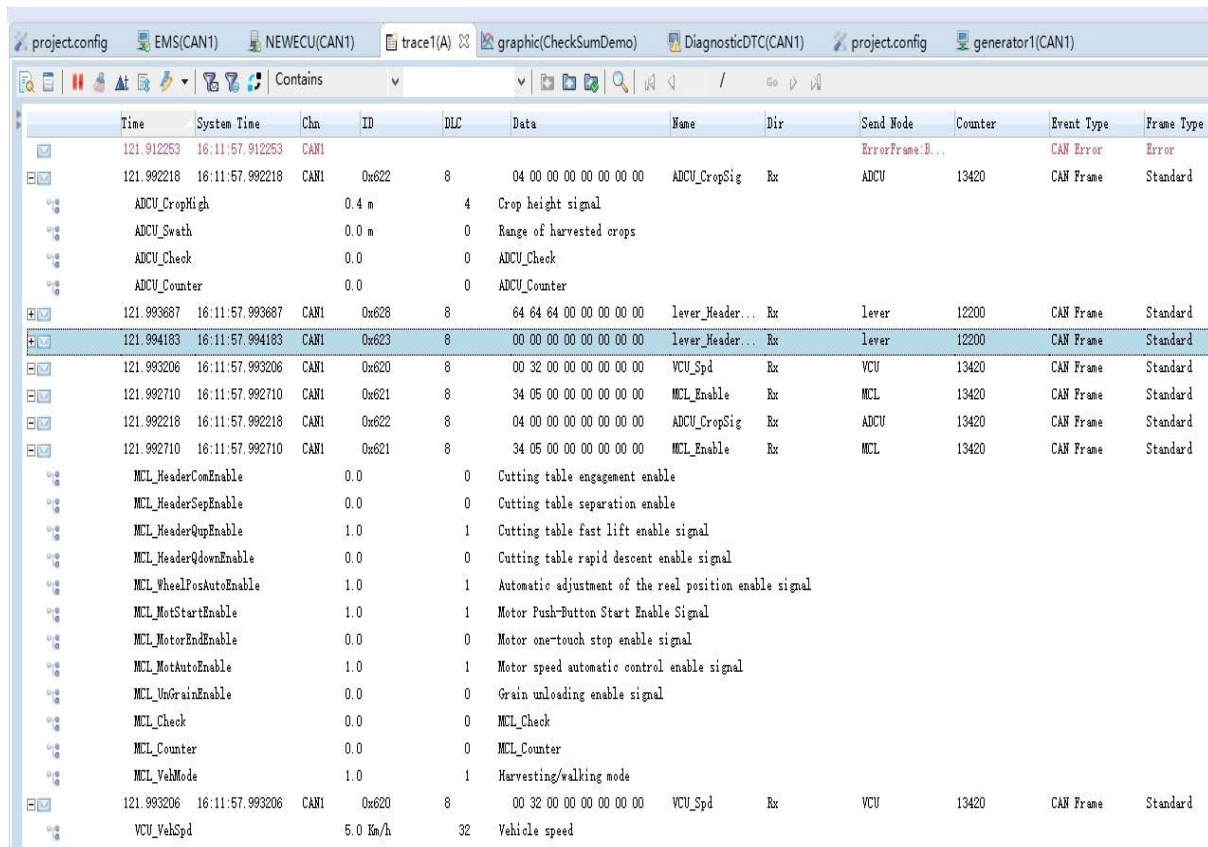
Fig. 3 - CAN communication real-time monitoring messages

To verify the optimization effect of the whale optimization PID and traditional PID control in regulating the lift of the cutting table, the dynamic response of the system will be observed. The mathematical transfer function for the lift of the cutting table is established. The opening of the reversing valve directly influences the speed of the hydraulic cylinder's lifting. The hydraulic cylinder's speed changes in accordance with the variation in the valve opening. The acceleration and deceleration, as well as the expansion and contraction of the hydraulic cylinder, are considered inertial elements (*Qin et al., 2009*). The transfer function for this process can be expressed as follows:

$$G(s) = \frac{1}{Ts+1}$$
(17)

where s is the Laplace operator, s^{-1}; T is the hydraulic cylinder inertia constant, s, here take 0.83.

The simulation model of the control strategy is built in Matlab/Simulink environment and its model diagram is shown in Figure 4.
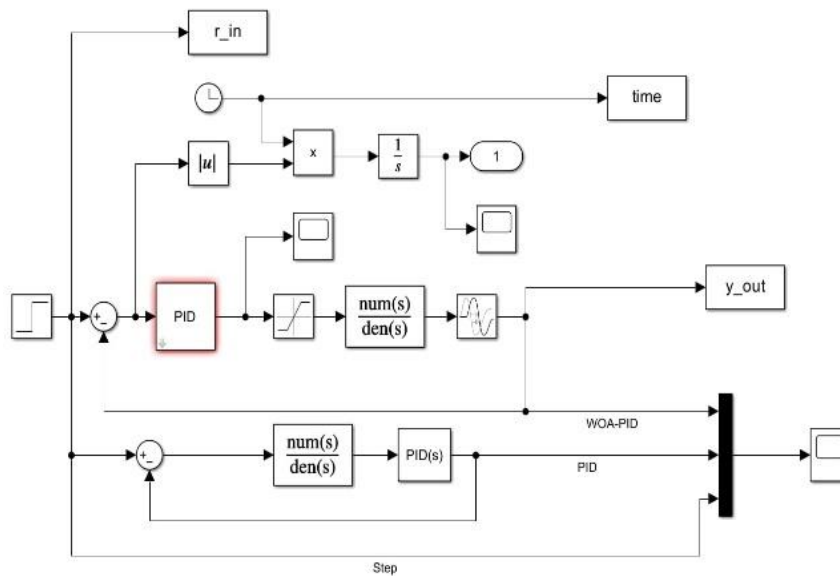

Fig. 4 - WOA-PID Simulink model

A step signal is used as the input to the system. After 10 iterations of the whale optimization algorithm, the optimal solution is obtained, yielding the corresponding values of Kp, Ki, and Kd. A comparison curve between the results of the optimized PID and the standard PID is then generated, and the resulting graph is shown in Figure 5.
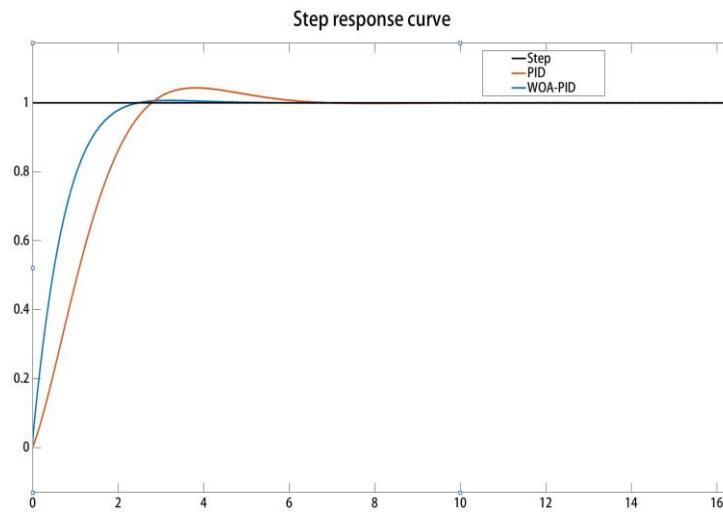
Fig. 5 - Control strategy step response comparison curve

From the dynamic response curve, it can be observed that the regulation effect of the whale optimized PID is significantly improved compared to the standard PID. The overshoot is reduced by 3.5%, and the rise time is improved by 0.303 seconds, enhancing the system's speed and stability.

To verify the feasibility of the semi-physical simulation platform for controller testing, a control experiment was conducted using the platform to simulate the working process of the rice and wheat harvester. The experimental indices included vehicle speed, cutting platform height, reel height and rotational speed, and auger rotational speed. These parameters were used to assess the accuracy and feasibility of the platform. The experiment was conducted in Junan County, Linyi City, Shandong Province, in a field of wheat to be harvested. The wheat had a grain height of approximately 450 mm, row spacing of about 300 mm, and a ground undulation of around 60 mm, with a uniform crop density across the field. The actual field measurements are shown in Figure 6. Based on the field conditions, the stubble height was set to 200 mm, and both the field experiment and semi-physical simulation platform experiment were carried out sequentially. According to the actual situation in the field, the stubble height was set to 200 mm, and the field experiment and semi-physical simulation platform experiment were carried out in turn.

| (a) plant height | (b) spacing |

Fig. 6 - Control strategy step response comparison curve

During field experiments, the harvester is set to harvesting mode, with the stubble height adjusted to 200 mm. The driving speed is increased to 12 km/h and maintained at a steady pace. As the terrain changes, the height of the cutting platform dynamically adjusts based on the detection values from the mimic device. The cutting platform's height is continuously recorded and using the mathematical relationship between the platform height and the angle sensor of the mimic device, the corresponding angle values are derived in response to terrain variations.

After harvesting a certain distance, the vehicle speed is reduced to 8 km/h. In harvesting mode, the rotational speeds of the reel and auger vary with the vehicle speed; therefore, the changes in rotational speed during acceleration and deceleration are recorded. The simulation platform parameters are configured based on the recorded angle values and vehicle speed from the field experiment. In the human-computer interaction interface, real-time monitoring is conducted to track the variations in cutting platform height in response to terrain changes, as well as the fluctuations in reel and auger rotational speeds corresponding to vehicle speed adjustments. The experimental results are presented in Table 2, Figure 7 and Figure 8.

As shown in Table 2, during the field test, the cutter height was recorded every 10 seconds from the actual vehicle and converted into the corresponding angular change as an input to the simulation platform. Throughout this process, the maximum absolute error in cutter height was 10.58 mm, which primarily resulted from conversion inaccuracies and voltage output errors from the platform. To evaluate the linear relationship between the actual cutter height and the simulated cutter height output from the platform, Pearson correlation analysis was conducted. The calculated Pearson correlation coefficient was 0.9474, indicating a strong correlation between the two. This result confirms that the simulation platform effectively replicates the cutter lifting and lowering process of the test vehicle.

The experimental results show that the rotational speeds of the reel and auger vary with the vehicle speed. Directly adjusting their speeds through the platform alone cannot fully ensure consistency with field measurements. To accurately control a single variable, the vehicle speed curve is pre-sampled and used as an input to the control strategy. However, the output speed curve from the simulation platform is influenced by factors such as the simulation step length and refresh period. Therefore, the generated curve must be exported for comparison with the actual speed curve. Compared to the harvester, the mathematical expectation of the rotational speed error for the reel and auger is 0.106 rad/min and 0.101 rad/min, respectively, with standard deviations of 0.165 rad/min and 0.172 rad/min. These results indicate that the control strategy meets the actual harvesting requirements. Moreover, the simulation platform provides an accurate evaluation of the controller's functionality, making it a valuable reference for functional testing in the early stages of controller development.

Table 2

Sensor and simulation platform angle measurements

Experiment number	Calculated height of cutter trial	Calculated height of cutting table simulation	Absolute error in height above ground	Relative error in height above ground
	[mm]	[mm]	[mm]	[-]
1	203.0	205.1	2.1	0.010
2	201.3	200.5	0.8	0.003
3	205.7	207.2	1.5	0.007
4	200.9	200.5	0.4	0.002
5	197.4	198.9	1.5	0.008
6	201.3	200.2	1.1	0.005
7	204.6	205.1	0.5	0.002

Experiment number	Calculated height of cutter trial	Calculated height of cutting table simulation	Absolute error in height above ground	Relative error in height above ground
	[mm]	[mm]	[mm]	[-]
8	202.4	201.5	0.9	0.004
9	193.3	193.6	0.3	0.002
10	204.8	203.4	1.4	0.007
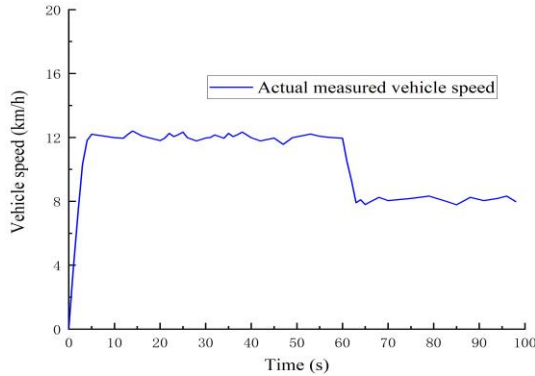
(a) Actual measured vehicle speed

(b) Simulated speed of the reel
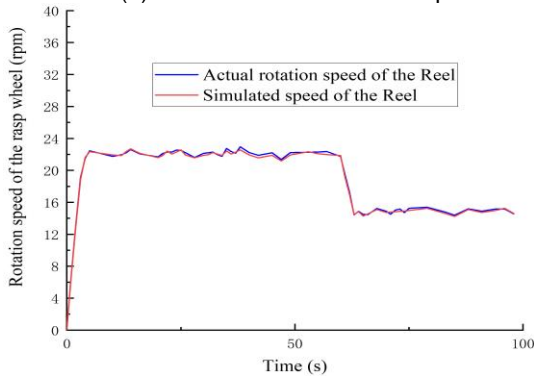
(c) Comparison of the reel speed
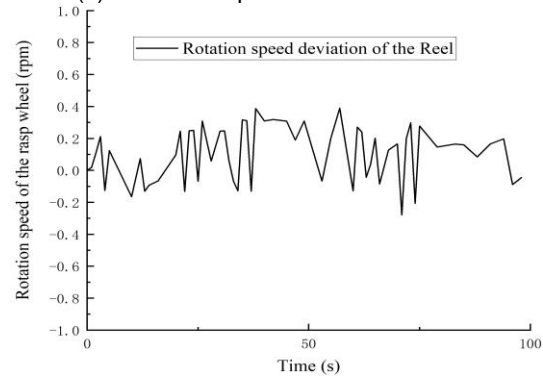
(d) Rotation speed deviation of the reel

Fig. 7 - Comparison curve between simulation and actual rotation speed of the reel
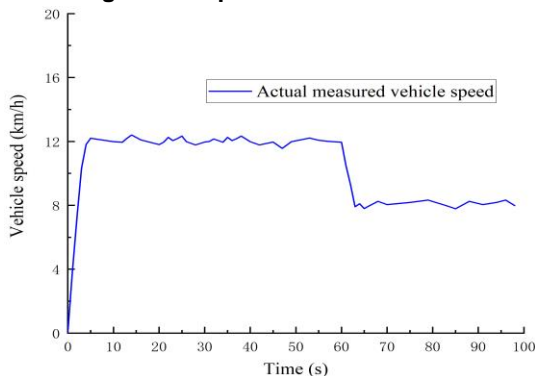
(a) Actual measured vehicle speed

(b) Simulated speed of the auger
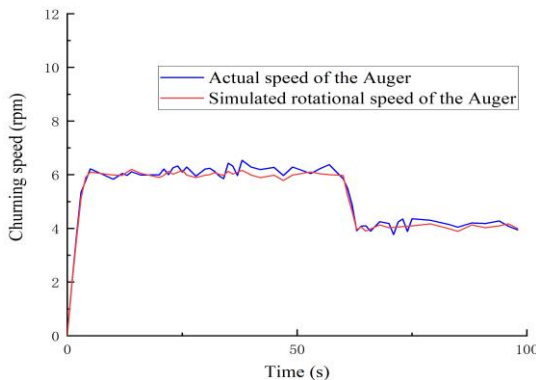
(c) Comparison of the auger speed
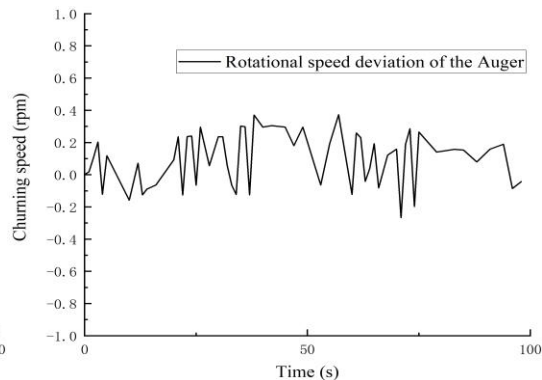
(d) Rotation speed deviation of the auger

Fig. 8 - Comparison curve between simulation and actual rotation speed of the auger

CONCLUSIONS

(1) To enhance the output response characteristics of the cutter height regulation strategy, the cutter controller is optimized by combining the Whale Optimization Algorithm with PID control. The simulation results demonstrate that the optimized PID controller reduces the overshoot by 3.5% compared to the conventional PID controller and improves the rise time by 0.303 seconds. These improvements indicate that the optimized control strategy can effectively regulate the cutter height with both stability and rapidity.

(2) To effectively evaluate the controller's performance under real physical signals, hardware-in-the-loop (HIL) tests were conducted on a semi-physical simulation platform. Angle sensor variations caused by terrain undulations were used as input variables, while the output height values of the platform and the field-measured cutter height values served as comparison control experiments. The results showed that the maximum absolute error between the simulated and measured height variations was 10.58 mm. This indicates that the developed cutting platform model has a strong correlation with the actual cutting platform mechanism and can serve as a reliable basis for pre-testing the cutting platform controller.

(3) When testing control strategies for reel speed and auger speed, the speed values are influenced by the vehicle speed. First, the vehicle speeds, along with the corresponding reel and auger speeds, are recorded during the field experiment. These recorded speeds are then used as input variables for the semi-physical simulation platform, which outputs the corresponding reel and auger speeds. By comparing the deviation between the actual values and the output values of the platform under the same vehicle speed input, it is found that the mathematical expected error for the reel speed is 0.106 rad/min, and for the auger speed, it is 0.101 rad/min. The standard deviations are 0.165 rad/min and 0.172 rad/min, respectively. These results validate the reliability and feasibility of the simulation platform and provide a theoretical foundation for the development and testing of the cutting platform control system.

REFERENCES

[1] Abboush, M., Knieke, C., & Rausch, A. (2024). A Virtual Testing Framework for Real-Time Validation of Automotive Software Systems Based on Hardware in the Loop and Fault Injection. *Sensors,* Vol. 24, pp. 3733, Germany.

[2] Cevallos, G., Herrera, M., & Jaimez, R. (2022). A Practical Hybrid Control Approach for a Greenhouse Microclimate: A Hardware-in-the-Loop Implementation. *Agriculture,* Vol. 12, pp. 1916, Ecuador.

[3] Chen, J., Wang, S., Lian, Y. (2018). Design and test of header parameter keys electric control adjusting device for rice and wheat combined harvester (稻麦联合收获机割台参数按键电控调节装置设计与试验). *Transactions of the Chinese Society of Agricultural Engineering,* Vol. 34, pp. 19-26, Jiangsu/China.

[4] Hang, Q., Hu, C., & Li, R. (2024). Research on Distributed Dual-Wheel Electric-Drive Fuzzy PI Control for Agricultural Tractors. *Agriculture,* Vol. 14, pp. 1442, Shandong/China.

[5] Ji, K., Li, Y., & Liang, Z. (2022). Device and Method Suitable for Matching and Adjusting Reel Speed and Forward Speed of Multi-Crop Harvesting. *Agriculture,* Vol. 12, pp. 213, Jiangsu/China.

[6] Ji, K., Li, Y., Ji, B., Liang, Z., & Du, T. (2023). Discrete element method used to analyze the operating parameters of the cutting table of crawler self-propelled reed harvester. *INMATEH - Agricultural Engineering,* Vol. 71, pp. 345-355, https://doi.org/10.35633/inmateh-71-30

[7] Klionovska, K., & Burri, M. (2021). Hardware-in-the-Loop Simulations with Umbra Conditions for Spacecraft Rendezvous with PMD Visual Sensors. *Sensors,* Vol. 21, pp. 1455, Germany.

[8] Liu, W., Luo, X., Zeng, S. (2022). Performance test and analysis of the self-adaptive profiling header for ratooning rice based on fuzzy PID control (基于模糊 PID 控制的再生稻自适应仿形割台性能试验与分析). *Transactions of the Chinese Society of Agricultural Engineering,* Vol. 38, pp. 1-9, Guangdong/China.

[9] Lu, K., Feng, G., & Ding, B. (2023). Robust H-Infinity Tracking Control for a Valve-Controlled Hydraulic Motor System with Uncertain Parameters in the Complex Load Environment. *Sensors,* Vol. 23, pp. 9092, Shenzhen/China.

[10] Miao, F., Wu, Y., & Yan, G. (2025). Dynamic multi-swarm whale optimization algorithm based on elite tuning for high-dimensional feature selection classification problems. *Applied Soft Computing,* Vol. 169, pp. 112634-112634, Shanghai/China.

[11] NadimiShahraki, M. H., Zamani, H., & Asghari, V. Z. (2021). A Systematic Review of the Whale Optimization Algorithm: Theoretical Foundation, Improvements, and Hybridizations. *Archives of Computational Methods in Engineering,* Vol. 30, pp. 106727, Australia.

[12]   Qin, Y., Zhao, D., Li, F. (2009). Constant Palstance Control of Combine Cylinder Based on RBF (基于 RBF 网络的联合收获机脱粒滚筒恒速控制). *Transactions of the Chinese Society for Agricultural Machinery,* Vol. 40, pp. 59-63, Jiangsu/China.

[13]   Shahir, F. M., Gheisarnejad, M., Sadabadi, M. S., & Khooban, M. H. (2021). A New Off-Board Electrical Vehicle Battery Charger: Topology, Analysis and Design. *Designs,* Vol. 5, pp. 51, Iran.

[14]   Shi, M., Li, Y., & Pan, Y. (2024). Design of an Adaptive Height Control System for Sugarcane Harvester Header. *Agronomy,* Vol. 14, pp. 1644, Guangxi/China.

[15]   Wei, F., Li, J., & Zhang, Y. (2023). Improved neighborhood search whale optimization algorithm and its engineering application. *Soft Computing,* Vol. 27, pp.17687-17709, China.

[16]   Wu, Z., Wang, J., & Xing, Y. (2023). Energy Management of Sowing Unit for Extended-Range Electric Tractor Based on Improved CD-CS Fuzzy Rules. *Agriculture,* Vol. 13, pp. 1303, Hubei/China.

[17]   Yao, J., Zhang, G., Wang, X., Lian, J., Liu, M., Qian, X., Wang, Y., & Liu, P. (2023). Harvest loss test and optimisation of key components of oilseed rape cutting tables. *INMATEH - Agricultural Engineering,* Vol. 71, pp. 429-440, https://doi.org/10.35633/inmateh-71-37

[18]   Yan, Z., Zhang, J., & Zeng, J. (2022). Three-dimensional path planning for autonomous underwater vehicles based on a whale optimization algorithm. *Ocean Engineering,* Vol. 250, pp. 111070, Harbin/China.

[19]   Zhao, Z., Shui, D., Liu, F., Zhao, B., & Wang, Z. (2024). Research regarding agricultural bionic blade development based on the mechanism of the cutting-sawing motion of the Camponotus mandible. *INMATEH - Agricultural Engineering,* Vol. 73, pp. 870-880, https://doi.org/10.35633/inmateh-73-73

[20]   Zhai, Z., Chen, Y., Zhu, S. (2023). Experiment on Electro-hydraulic Hitch Control System for Hilly and Mountainous Tractor Based on Semi-physical Simulation (基于半实物仿真的丘陵山地拖拉机电液悬挂控制试验). *Transactions of the Chinese Society for Agricultural Machinery,* Vol. 53, pp. 328-337, Beijing/China.

[21]   Zhu, X., Chi, R., Du, Y. (2022). Design of Hardware in Loop Simulation Platform for Intelligent Control System of Corn Kernel Harvester (玉米收获机低损脱粒智能控制系统半实物仿真平台设计). *Transactions of the Chinese Society for Agricultural Machinery,* Vol. 53, pp. 114-122, Beijing/China.